https://doi.org/10.59849/2219-6641.2026.1.15

PALEOSEISMOLOGY OF THE SHIRVAN STRIKE-SLIP FAULT SYSTEM

N. Marshall[1], G.J. Yetirmishli[2], S.E. Kazimova[2], I. Pierce[1], R. T Walker[1], B. Johnson[1], I.E. Kazimov[2], G. P. De Pascale[3], I. Guliyev[4]

neill.marshall@worc.ox.ac.uk, sabina.k@mail.ru, i.pearce@manchesterurology.org.uk, richard.walker@earth.ox.ac.uk, benedict.johnson@st-annes.ox.ac.uk, ilya_24@mail.ru, gregoryp@hi.is, *ibrahim.guliyev*@science.az.

Abstract

This study presents the results of an integrated geomorphological, structural, and paleoseismological investigation of the Shirvan strike-slip fault zone, located within the Kura–Araz Depression at the western margin of the South Caspian Basin (Azerbaijan). Using high-resolution Pléiades satellite stereo imagery, UAV aerial photography, field mapping, and digital elevation models, we identified evidence of active right-lateral strike-slip deformation, including offset river channels, terrace scarps, compression and extension zones, as well as pop-up and pull-apart structures. A close spatial relationship between the fault trace, anticlinal folding, and the linear distribution of mud volcanoes indicates structural control over their formation.

For the first time, paleoseismological studies of the Shirvan Fault were carried out by excavating two trenches near Salyan. Stratigraphic analysis combined with infrared luminescence (IRSL) and radiocarbon dating allowed reconstruction of the paleoseismic history over the past ~3000 years. Four to six surface-rupturing events were identified with irregular recurrence intervals averaging 500–750 years, including a clustering of 2–3 events in the last ~500–600 years. The minimum geological slip rate along the fault was estimated at 3.9–4.8 mm/yr during the Holocene.

Considering the fault zone length of ~150 km, inferred from geomorphology, seismicity, and mud volcano distribution, a full rupture could generate an earthquake of up to Mw ~7.5. However, the absence of large historical earthquakes and the nature of faulting within fluid-saturated sediments of the Kura–Araz Depression suggest that part of the deformation may occur aseismically or as triggered events. These results highlight the key role of the Shirvan strike-slip zone in the current tectonics of the South Caspian

Keywords: Paleoseismology, Shirvan Strike-Slip Fault, West Caspian Fault, seismic hazard assessment, active tectonics, South Caspian Basin, Azerbaijan

ŞİRVAN SAĞ-TƏRƏFLİ QIRILMA SİSTEMİNİN PALEOSEİSMİK TƏHLİLİ

N.Marşal, Q.C.Yetirmişli, S.E.Kazımova, I.Piirs, R.T.Volker, B.Johnson, I.E.Kazımov, G.P.De Pascal, I.Quliyev

Xülasə

Bu tədqiqat, Cənubi Xəzər hövzəsinin (Azərbaycan) qərb kənarında, Kür-Araz çökəkliyində yerləşən Şirvan strike-sürüşmə qırılma zonasının inteqrasiya olunmuş geomorfoloji, struktur və paleoseismoloji tədqiqatının nəticələrini təqdim edir. Yüksək qətnaməli Pléiades peyk stereo görüntülərindən, PUA hava fotoqrafiyasından, sahə xəritələşdirməsindən və rəqəmsal yüksəklik modellərindən istifadə edərək, ofset çay kanalları, terras çuxurları, sıxılma və uzanma zonaları, eləcə

[1] COMET, Department of Earth Sciences, Oxford University, Oxford, OX1 3AN, UK
[2] Republican Seismic Survey Center of Azerbaijan National Academy of Science, Baku, Azerbaijan
[3] School of Engineering and Natural Sciences, University of Iceland, Reykjavík, Iceland.
[4] Azerbaijan National Academy of Science, Baku, Azerbaijan.

də açılan və ayrılan strukturlar da daxil olmaqla, aktiv sağ tərəfli zərbə-sürüşmə deformasiyasının sübutlarını müəyyən etdik. Qırılma izi, antiklinal qatlanma və palçıq vulkanlarının xətti paylanması arasında sıx məkan əlaqəsi onların əmələ gəlməsi üzərində struktur nəzarətini göstərir.

İlk dəfə olaraq Şirvan qırılmasının paleoseismoloji tədqiqatları Salyan yaxınlığında iki xəndək qazmaqla aparılmışdır. İnfraqırmızı lüminesans (IRSL) və radiokarbon tarixləndirməsi ilə birləşdirilmiş stratiqrafik analiz son ~3000 il ərzində paleoseismik tarixin yenidən qurulmasına imkan vermişdir. Son ~500-600 ildə 2-3 hadisənin klasterləşməsi də daxil olmaqla, orta hesabla 500-750 il davam edən qeyri-müntəzəm təkrarlanma intervalları ilə dörd-altı səth yırtığı hadisəsi müəyyən edilmişdir. Holosen dövründə qırılma boyunca minimum geoloji sürüşmə sürəti ildə 3,9-4,8 mm olaraq qiymətləndirilmişdir.

Geomorfologiya, seysmiklik və palçıq vulkanlarının paylanmasından əldə edilən təxminən 150 km uzunluğunda qırılma zonası nəzərə alındıqda, tam qırılma Mw ~7.5-ə qədər zəlzələ yarada bilər. Lakin, böyük tarixi zəlzələlərin olmaması və Kür-Araz çökəkliyinin maye ilə doymuş çöküntülərində qırılmaların təbiəti deformasiyanın bir hissəsinin seysmik və ya tetiklenen hadisələr kimi baş verə biləcəyini göstərir. Bu nəticələr Cənubi Xəzərin hazırkı tektonikasında Şirvan zərbə-sürüşmə zonasının əsas rolunu vurğulayır.

Açar sözlər: Paleoseizmologiya, Şirvan sağ-tərəfli qırılması, Qərb Xəzər Qırılması, seysmik risk qiymətləndirilməsi, aktiv tektonika, Cənubi Xəzər Bazası, Azərbaycan

Аннотация

В данном исследовании представлены результаты комплексного геоморфологического, структурного и палеосейсмологического исследования зоны Ширванского сдвигового разлома, расположенной в пределах Кура-Аразской впадины на западной окраине Южно-Каспийского бассейна (Азербайджан). Используя стереоизображения со спутника Pléiades высокого разрешения, аэрофотосъемку с БПЛА, полевое картирование и цифровые модели рельефа, мы выявили свидетельства активной правосторонней сдвиговой деформации, включая смещенные русла рек, террасовые уступы, зоны сжатия и растяжения, а также структуры поднятия и раздвигания. Тесная пространственная взаимосвязь между следом разлома, антиклинальной складчатостью и линейным распределением грязевых вулканов указывает на структурный контроль их формирования.

Впервые были проведены палеосейсмологические исследования Ширванского разлома путем раскопок двух траншей вблизи Сальяна. Стратиграфический анализ в сочетании с инфракрасной люминесценцией (ИКЛ) и радиоуглеродным датированием позволил реконструировать палеосейсмическую историю за последние ~3000 лет. Было выявлено от четырех до шести событий разрыва поверхности с нерегулярными интервалами повторяемости в среднем 500–750 лет, включая кластеры из 2–3 событий за последние ~500–600 лет. Минимальная геологическая скорость смещения вдоль разлома оценивалась в 3,9–4,8 мм/год в течение голоцена.

Учитывая длину зоны разлома около 150 км, определенную на основе геоморфологии, сейсмичности и распределения грязевых вулканов, полный разрыв мог бы вызвать землетрясение магнитудой до Mw ~7,5. Однако отсутствие крупных исторических землетрясений и характер разломообразования в насыщенных жидкостью отложениях Кура-Аразской впадины позволяют предположить, что часть деформации могла происходить асейсмически или в виде триггерных событий. Эти результаты подчеркивают ключевую роль Ширванской сдвиговой зоны в современной тектонике Южного Каспия.

Ключевые слова: Палеосейсмология, Ширванский сдвиговый разлом, Западно-Каспийский разлом, оценка сейсмической опасности, активная тектоника, Южно-Каспийский бассейн, Азербайджан.

Introduction

Active strike-slip faulting in low-relief basins presents a persistent challenge for tectonic and seismic studies, particularly in regions with complex interactions between sedimentation, folding, and volcanism. The Kura Basin, situated at the western edge of the South Caspian region, is characterized by a combination of low-gradient topography, extensive sedimentary cover, and active mud-volcanic activity, which together obscure direct geomorphic evidence of faulting. Despite decades of regional seismic monitoring and geological investigation, the kinematics, slip history, and paleoseismic behavior of key faults within the basin remain poorly constrained, limiting our ability to assess earthquake hazards in eastern Azerbaijan.

Among these structures, the Shirvan fault zone has been proposed based on regional geomorphology, alignment of mud volcanoes, and localized seismicity patterns. However, detailed quantitative field studies that integrate modern remote sensing techniques with paleoseismological data have been largely absent. Understanding the behavior of this fault is critical, not only for regional seismic hazard assessment but also for improving models of strike-slip deformation and crustal strain distribution within the Kura Basin and adjacent Caucasus region.

In this study, we employ a multi-disciplinary approach to characterize the Shirvan fault zone and associated structures. High-resolution satellite imagery from the Pléiades mission, combined with structure-from-motion (SfM) surveys using UAVs, allows us to generate digital elevation models (DEMs) with sub-meter resolution, enabling detailed mapping of fault scarps, offset drainage channels, and terrace risers. Field-based geomorphic mapping and paleoseismic trenching provide independent verification of fault locations, as well as constraints on displacement and recurrence of past surface-rupturing earthquakes. Quaternary dating techniques, including radiocarbon and infra-red stimulated luminescence (IRSL), are used to bracket the timing of past seismic events and to estimate the long-term slip-rate of the fault.

By integrating remote sensing, field observations, and chronological data, this study provides a comprehensive assessment of the Shirvan fault zone, offering new insights into its geometry, kinematics, and seismic potential. The findings contribute to a better understanding of active right-lateral strike-slip faulting in the Kura Basin, highlighting the relationships between faulting, mud-volcanism, and regional tectonics, and provide critical data for improving earthquake hazard models in eastern Azerbaijan.

The Kura Basin.

The Shirvan fault zone is located within the Kura Basin, a structural depression situated between the Greater Caucasus to the north and the Lesser Caucasus to the south. The basin contains a sedimentary sequence estimated at ~15 km thick (Piip et al., 2012), overlying a granitic-metamorphic basement (Nadirov et al., 1997). Eastern Azerbaijan hosts numerous mud volcanoes distributed both onshore within the Kura Basin and offshore in the South Caspian Basin. These muds originate primarily from the Oligocene Maykop Formation, which underlies approximately 10 km of productive sand series (Abdullayev et al., 2017; Allen et al., 2002; Mangino & Priestley, 1998; Piip et al., 2012). Mud volcanism is driven by overpressured sediments and hydrocarbons, compounded by tectonic compression from the Arabia-Eurasia collision, resulting in elevated pore pressures within the basin (Feyzullayev et al., 2015; Mazzini & Etiope, 2017).

Crustal thickness in the Kura Basin decreases eastward from ~60 km in the west to ~45 km near the South Caspian Basin boundary (Mangino & Priestley, 1998). The eastward-flowing Kura River promotes high sedimentation rates in the basin today. Active deformation occurs along the Kura fold-and-thrust belt and the Greater Caucasus, with reverse faulting concentrated along frontal thrusts (Fig. 1) (Allen et al., 2004; Copley & Jackson, 2006; Forte et al., 2010, 2013; Gunnels et al., 2020; Jackson et al., 2002). GNSS measurements indicate northward motion of the Kura Basin relative to Eurasia at 13.2 ± 0.5 mm/yr (Kadirov et al., 2012; Reilinger et al., 2006) (Fig. 2).

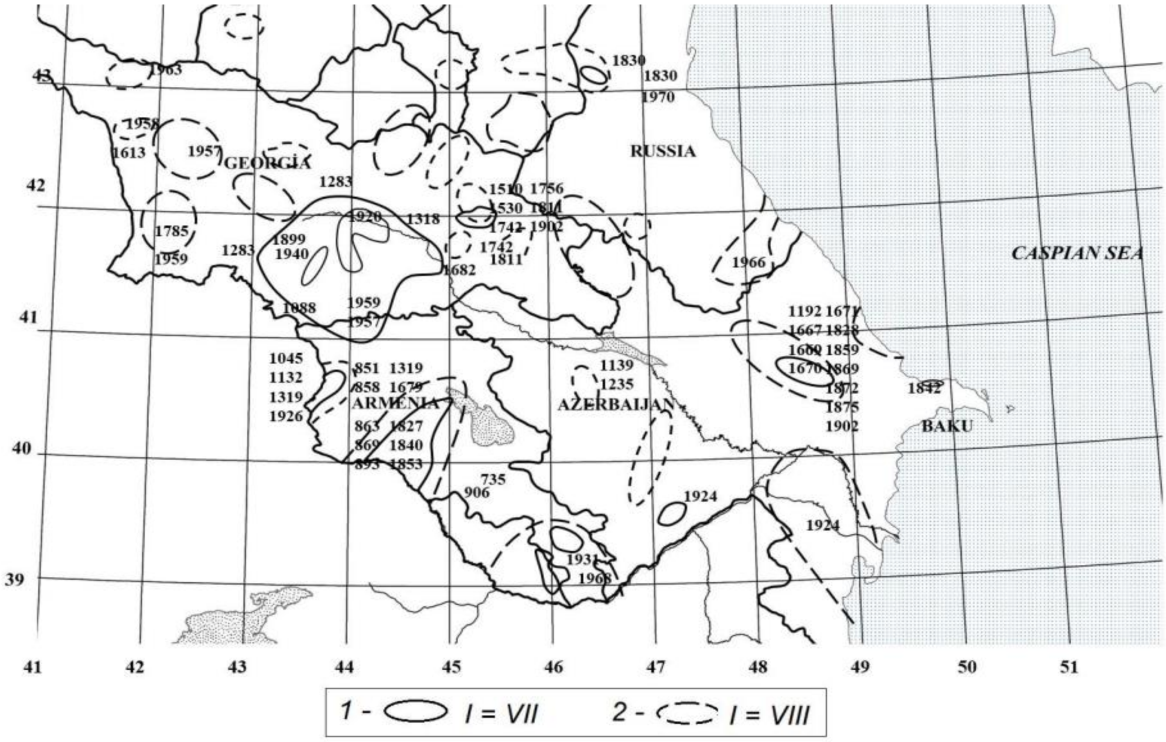

Fig. 1. Spatial Distribution of Epicenters of Strong Earthquakes (M > 6.0) in the Caucasus Region from 427 to 2024 CE, Showing Active Fault Zones and Seismic Clusters

Most well-recorded earthquakes in the Kura Basin are moderate in magnitude and occur at depths exceeding 10 km (Copley & Jackson, 2006; Gunnels et al., 2020; Jackson et al., 2002, 2021; Engdahl et al., 2006). Historically, the Shirvan fault zone exhibits evidence of larger events, with earthquakes exceeding magnitude 6 recorded in eastern Azerbaijan and adjacent regions during the period 427–2025 CE. Notable events include the 1139 Shamakhi earthquake (M ~7.0), the 1667 Shamakhi earthquake (M 6.9), and the 1859 Baku-Shirvan earthquake (M ~6.2), which affected the Kura Basin and demonstrate the potential for high-magnitude surface-rupturing events along active faults in this area (Ambraseys & Melville, 1982; Shebalin & Leydecker, 1997). Although smaller events, such as the M 4.0 earthquake near Salyan in 1881 (intensity 5), are documented more precisely, the historical record is incomplete and likely underestimates the frequency of strong seismic events along the Shirvan fault.

Active faulting in Azerbaijan and the southeastern Caucasus is governed by north-south shortening within the Arabia-Eurasia collision zone and the independent motion of the South Caspian Basin (Jackson & McKenzie, 1984; Jackson et al., 2002). Understanding the tectonics of the adjacent South Caspian Basin is therefore essential for interpreting the kinematics and seismic potential of faults in eastern Azerbaijan. Additionally, sea-level fluctuations in the Caspian Sea have significantly influenced local geomorphology.

The South Caspian Basin (SCB)

The South Caspian Basin is bordered by the Kopeh Dagh, Alborz, and Talesh deforming belts to the east, south, and west, respectively, and by the Apsheron Ridge to the north. Seismic studies, including receiver functions and reflection profiles, indicate a low-velocity sedimentary layer 15–20 km thick overlying a high-velocity, basaltic-like layer (Jackson et al., 2002). Reinterpretation of seismic refraction data suggests a thinned crust of ~10 km and a Moho at ~35–40 km depth (Piip et al., 2012). The Miocene deposits begin at 8–9 km depth, while the upper 3 km consist of Quaternary sediments (Abdullayev et al., 2017; Allen et al., 2002).

The SCB is largely aseismic and appears to move independently of surrounding regions, with motion rates of 10.4 ± 1.1 mm/yr (direction 333° ± 5° relative to Eurasia) and 4.8 ± 0.8 mm/yr (direction 236° ± 14° relative to Iran) (Copley & Jackson, 2006; Djamour et al., 2010; Walker et al., 2021). Earthquakes north of the Apsheron Ridge, occurring at depths >80 km, are interpreted as subduction of the SCB basement beneath Eurasia (Jackson et al., 2002, 2021; Walker et al., 2021). Shallow-angle reverse faulting at depths up to 40 km beneath the Talesh and Kura Basin also suggests westward subduction. While some studies date the onset of subduction to 5.5 Ma, seismic line analysis points to an earlier, Miocene initiation (Allen et al., 2002; Green et al., 2006).

Relative motion of the SCB is accommodated along conjugate faults: dextral Main Kopeh Dagh Fault and sinistral Shahroud Fault zone (Dodds et al., 2022b; Hollingsworth et al., 2008). Faulting along the SCB's southern margin transitions from left-lateral slip in the east to increased shortening in the west along the Alborz range. GNSS data indicate northward motion of the Talesh and Kura basins at 10–13 mm/yr relative to Eurasia, with northeastward rotation and decreasing velocities between Salyan and Baku (Kadirov et al., 2012; Reilinger et al., 2006). Kinematic modeling suggests that N–S strike-slip motion is feasible (Djamour et al., 2010; Kadirov et al., 2012), with ~7.5 mm/yr relative motion between the SCB and the Turkish-Iranian Plateau and Kura Basin, resolved into 1.9 mm/yr right-lateral strike-slip and 7.2 mm/yr shortening along N–S structures (Dodds et al., 2022).

The structures accommodating SCB–Kura relative motion remain poorly constrained. North–south right-lateral earthquakes are documented in the Talesh region (e.g., Mw 6.1 Ardebil, 1997) alongside mapped right-lateral geomorphic offsets (Aziz Zanjani et al., 2013). Similar right-lateral and reverse faulting may extend across the Kura Basin, but rapid sedimentation complicates identification of active faults. Deep NNW–SSE seismicity trends (>30 km depth) suggest a dextral strike-slip West Caspian Fault (Gunnels et al., 2020), supported by sedimentary thickness changes (Allen et al., 2003) and gravity anomalies (Khain et al., 1966). Evidence of right-lateral shear and en echelon folds between Shirvan and Salyan has been reported (Trifonov, 1978; Allen et al., 2003; Khain et al., 1966), but confirmation across the Kura Basin remains uncertain (Copley & Jackson, 2006).

Methods

We employed a multi-scale approach combining remote sensing, UAV surveys, geomorphic mapping, paleoseismic trenching, and Quaternary dating to characterize fault activity along the Shirvan fault zone.

High-resolution stereo imagery from the Pléiades satellite (https://portal.opentopography.org/dataCatalog, 19/05/2021, SO21034807-2) was used to construct digital elevation models (DEMs) of onshore topography. Agisoft Metashape software allowed point matching and DEM generation at 1 m/pixel resolution. Faults were preliminarily mapped using hillshade images of the DEMs, Google Earth, and Bing Aerial imagery, guiding subsequent field investigations. Elevations were geoid-corrected using the emg2008-5 model (Karney, 2019).

Detailed UAV surveys were conducted near Salyan using a DJI Phantom 4 Pro v2 with Teokit dGPS for precise geolocation, processed into orthomosaics and DEMs at 2.6 cm/pixel resolution (Zhang et al., 2019). Field and UAV-derived data were combined for geomorphic and fault mapping. Fault scarps and displaced drainage channels were identified, and offsets measured using abandoned terrace risers and thalwegs as piercing lines. Measurements were performed in QGIS and refined using the LaDiCaoz Matlab program to restore drainage channels and terrace slopes (Zielke & Arrowsmith, 2012; Kurtz et al., 2018). Offsets near Shirvan were extracted from satellite-derived DEMs following the same principles, with minimum and maximum displacements estimated from nearby risers. Qualitative assessments of sinuosity, clarity, and obliquity provided uncertainty constraints.

Paleoseismic trenching comprised two trenches that were cleaned, gridded, photographed, and logged. Orthophoto mosaics derived from high-resolution photographs processed in Agisoft

Metashape and scaled with iPad-LiDAR reference points facilitated trench logging (Pierce & Koehler, 2023). Units, faults, and folds were distinguished following established paleoseismic protocols (McCaplin, 2009). Elevation profiles were measured using the Emlid Reach RS2 dGPS and corrected with the emg2008-5 geoid model. At Salyan, a 2.3 m deep sediment pit provided material for dating and constraints on slip history.

Quaternary dating involved both radiocarbon and infra-red stimulated luminescence (IRSL) analyses. Charcoal nodules from a burn layer at 2.1 m depth were radiocarbon-dated, along with a marine bivalve shell from Trench 1, at Beta Analytic (Miami, FL) and calibrated using OxCal v4.4 with the Marine20 curve and ΔR adjustment (-128) for the Caspian Sea (Bronk Ramsey, 1995). IRSL dating was applied to 23 sediment samples (17 from Trench 1, 3 from Trench 2, 3 from the sample pit), processed on single feldspar grains (Rhodes, 2015) with finite mixture modelling to identify dose groupings (Galbraith & Green, 1990). Only a subset of 13 samples was processed due to sufficient radiocarbon material from the pit.

The Shirvan Fault Zone

We identify three sections where the Shirvan fault is clearly expressed in the geomorphology, each associated with larger-scale features such as anticlinal folding and mud volcano activity. We infer that the fault zone continues between these segments, even where geomorphic expression is absent in the low-lying parts of the Kura Basin. Mud volcanoes are aligned along the fault trace, clustering near bends that coincide with local anticlinal structures. This alignment extends south of the visible fault ends, suggesting the fault is longer than indicated by surface features. Seismicity also follows a ~150 km NNW-SSE trend along the fault, with depths up to 40 km, extending from Shamakhi through Shirvan and Salyan, and continuing ~100 km offshore into the Caspian Sea.

East-facing scarps run along the apex of anticlinal hills and mud volcanoes south of Shamakhi, marked by brown triangles. No lateral offsets are observed here, although right-lateral slip is inferred based on features further south near Shirvan.

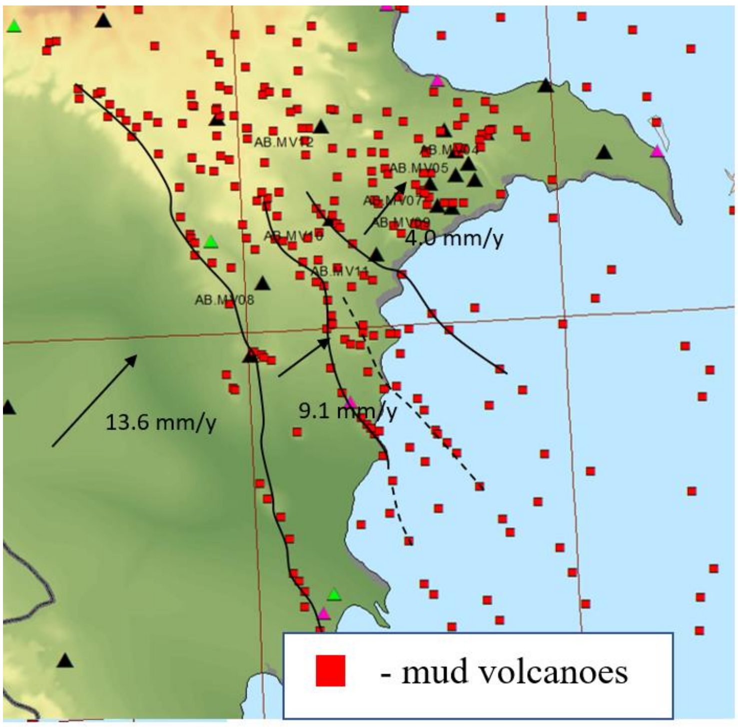

Fig. 2. Active faults in the Shirvan region and GNSS velocity vectors for the area. Red squares show the location of active mud volcanoes, black lines show the fault mapping in this study.

Near Shirvan, linear scarps cut across an anticline, with uphill-facing profiles. Several right-laterally offset drainages are present (Fig. 3), though the number of measurable offsets is insufficient for robust statistics. Stepovers along the fault include both left- and right-stepping segments (Fig. 3b & c). Left-stepping segments show an elevation increase bounded by rupture strands, indicative of right-lateral motion, while right-stepping zones show lowered elevations, consistent with transtension and right-lateral slip.

At Salyan, a linear fault trace bounds the western edge of a flat-topped uplifted area, interpreted as an eroded anticline formed during a sea-level highstand. Shelly marine terrace deposits are preserved locally on the surface.

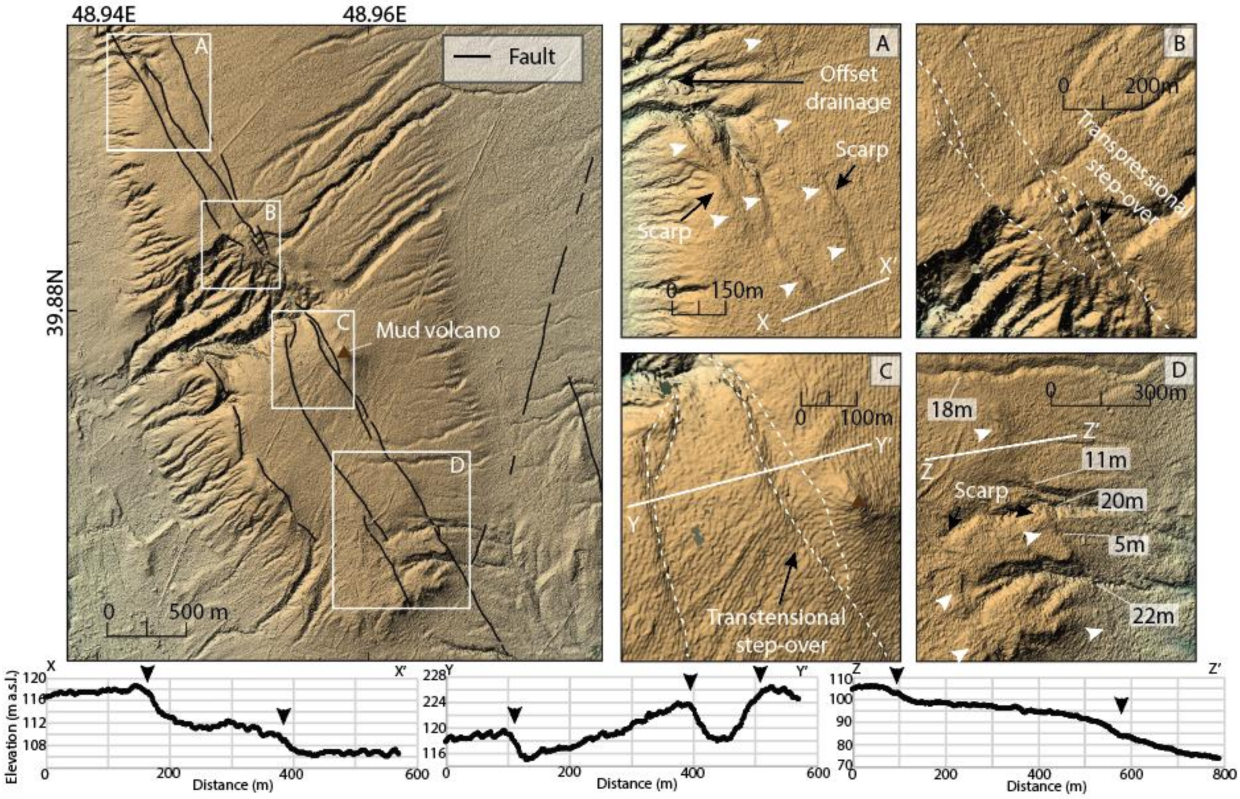

Fig. 3. Rupture map of the Shirvan fault zone. Panel D shows the main fault trace splitting into three strands, forming scarps visible in the topography; the topographic profile XX' highlights these scarps. An offset drainage is observed along the NW section of the rupture. Panel B illustrates the rupture trace with a transpressional step-over (pop-up) structure. Panel C shows scarps and a transtensional pull-apart basin associated with a step-over, as seen in topographic profile YY'. Panel D also displays two rupture traces with scarps and offset drainage channels, with measured offsets ranging from 5 to 22 m; scarps are highlighted in profile ZZ'.

The fault trace along the western side of the fold curves from nearly N–S in the north to NW–SE in the south, with the fold axis aligned parallel to the NW–SE segment. Small antithetic left-lateral faults offset the vertically dipping beds within the anticline.

In the field, the main fault trace follows an ~8 m-high scarp topped by a marine terrace. At this site, we conducted a UAV survey, excavated paleoseismic trenches, and opened a soil pit in the adjacent terrace. UAV-derived DEMs and field mapping reveal right-lateral offsets of terrace risers of 8 m and 54 m across the main fault. Additional southeastward drainages along the fault show dextral displacements, mostly ranging between 7–10 m.

Paleoseismology of the Shirvan Fault

To investigate the paleoseismic history and determine slip rates along the Shirvan Fault, two trenches were excavated, each revealing complex stratigraphy, fault structures, and Quaternary deposits. This allowed us to correlate geomorphic surfaces with dated sedimentary layers and reconstruct the history of fault activity.

Trench 1

Trench 1 is 18 m long and 3 m deep from the top of the scarp to the base of the excavation. The stratigraphy comprises four facies:

Facies 1 includes the basal deposits — chocolate clays (U10) and blue sands (U20). These layers, lying horizontally or on a slight slope, form the foundation of the stratigraphic sequence.

Facies 2 is located between two vertical fracture zones and includes units U50, U60, and U65 — coarse to medium sands containing intact shells, indicative of nearshore or beach environments. Salt layers in U60 and U65 are observed leaching from trench walls, suggesting ancient groundwater influence.

Facies 3 consists of fluvial/alluvial deposits, including U30, U40, U45, U70, U80, and U130, with grain sizes ranging from fine sands to silts. Channel structures within U30 and U40 cut into older layers, indicating sediment transport from the marine terrace (Qmt) above.

Facies 4 consists of massive silts (U85–U120), interpreted as wind-blown deposits accumulating at the base of the scarp.

Two vertical fracture zones cross the trench, forming a flower structure and local 0.5 m high pop-up features, with layer offsets and angular unconformities between facies. These fractures indicate right-lateral strike-slip faulting. UAV-derived DEMs and field mapping reveal terrace riser offsets of 8–54 m, confirming significant dextral motion along the fault.

Trench 2

Trench 2, 11 m long and 1.5 m deep, exposes the fluvial T1 terrace. Stratigraphy consists of a single facies comprising seven units, fining upward.

Lower units (U1–U3) include medium to coarse sands with pebble layers and salts, recording active fluvial deposition.

Middle units (U4–U5) contain finer laminated sands, partially offset by vertical fractures.

Upper units (U6–U7) are laminated silts and blocky soils, marking the cessation of sedimentation and formation of modern surfaces.

Two vertical fracture zones disrupt U1–U5, with the eastern zone reaching the current surface, representing the most recent earthquake (MRE). Overlying layers cap the fractures, recording two earlier seismic events, yielding a total of three paleoseismic events identified from this trench.

Age control.

Infrared-stimulated luminescence (IRSL) dating was used due to limited organic material for radiocarbon dating. In Trench 1, U50 yielded an age of 4520 ± 280 BP, while marine shells from U65 dated to ~14,100–14,900 cal. BP. Correlations between Trench 2 and a nearby sample pit link fluvial and slope deposits chronologically. The 7.5 m offset of the Qt3 terrace riser is constrained to ~2850 ± 310 to 350 ± 50 years BP, providing a key estimate for the long-term slip rate along the Shirvan Fault.

Our paleoseismic investigations along the Shirvan Fault, combining observations from Trenches 1 and 2, reveal evidence of multiple surface-rupturing events over the last ~3000 years. Based on IRSL dating and stratigraphic correlations, we identify at least four well-constrained events, with the possibility of three additional events (Fig. 4). While IRSL ages are stratigraphically consistent, they are younger than radiocarbon ages from marine shells at deeper levels, suggesting that some age brackets may underestimate the true timing of older events.

Paleo-earthquakes and Slip Rate of the Shirvan Fault Zone

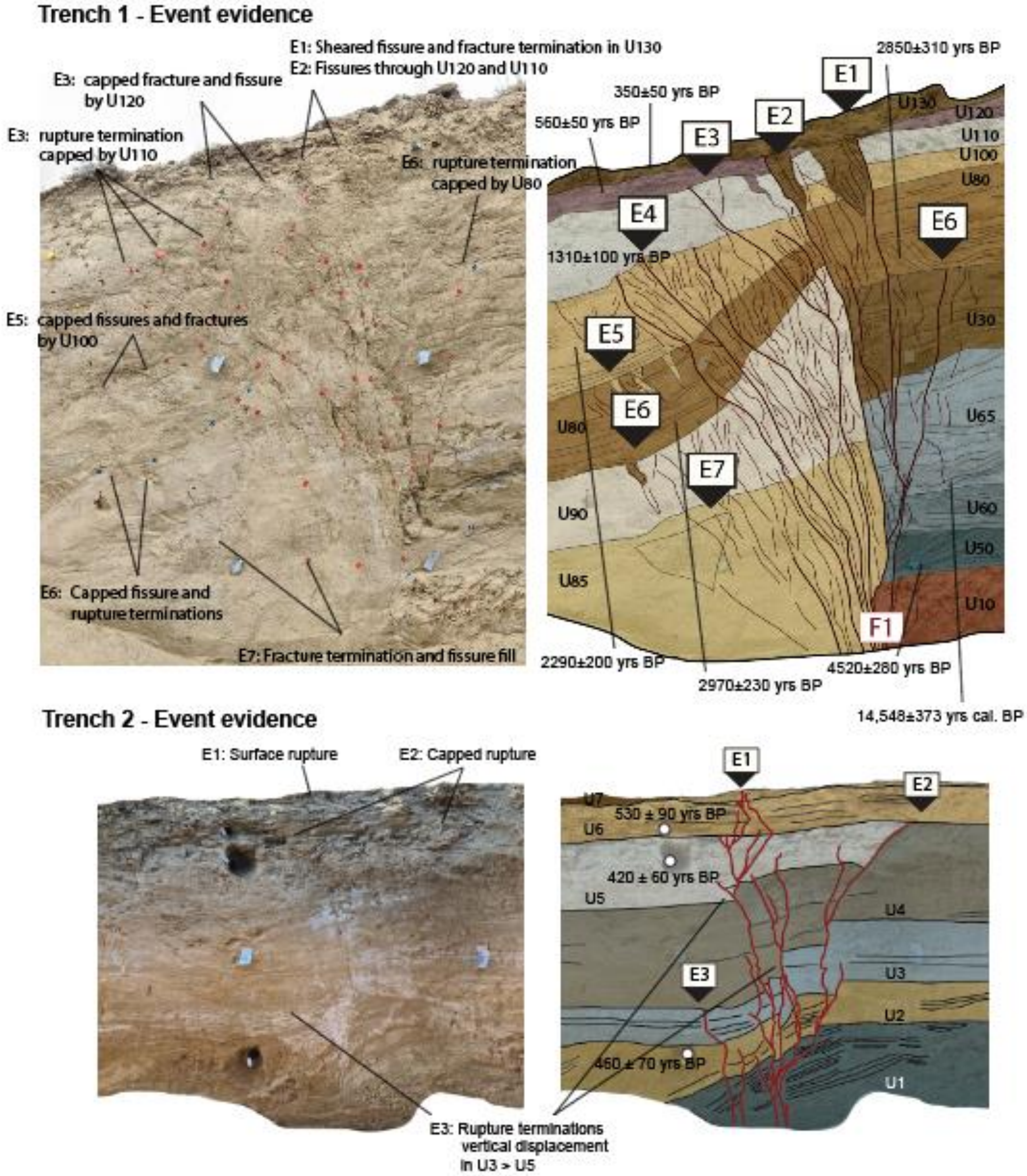

Fig. 4. Event evidence from trenches 1 and 2. Units and event labels are consistent with the trench logs. Trench 1 has evidence for at least 4 and up to 7 events. Ages are from IRSL and radiocarbon dating techniques.

The most recent surface-rupturing earthquake (Event 1) is constrained to 350 ± 50 years BP in Trench 1 and 530 ± 90 years BP in Trench 2. No clear offsets were observed across terrace risers at the trench site, though two small dextral offsets (<3 m) at Salyan may relate to this event. Event 2 is recorded as fissure fills in Trench 1 (U130, 350 ± 50 years BP) and capped fault terminations in Trench 2 (440–480 years BP). Event 3 is indicated by capped layers in Trench 1 (U120, 560 ± 50 years BP) and corresponding fault terminations in Trench 2 (420–460 years BP).

Older events include Event 4, bounded between 1310 ± 100 and 2290 ± 200 years BP, represented by capped fissures in Trench 1 (U110–U100). Event 5, at the boundary of U100 and U80 in Trench 1, is constrained between 2290 ± 200 and 2970 ± 230 years BP based on sealed fractures. Event 6 involves fractures capped by the base of U80, with IRSL ages of 2850–2970 years BP, indicating a probable age of 2740–3160 years BP. Event 7, inferred from capped fissures at the base of F1, lacks sufficient age control and is excluded from recurrence estimates.

Combining both trenches, we estimate 4–6 surface-rupturing earthquakes in the past 3000 years, corresponding to an average recurrence interval of ~500–750 years. However, events are temporally clustered, with 2–3 occurring within the last 500 years, while older events are more widely spaced.

The long-term slip rate of the Shirvan Fault is constrained using the right-lateral offset of 53 ± 4 m between the Qad (upper) and Qt2 (lower) terraces. Charcoal samples from the Qad terrace yield ages of 1744–2145 cal. BP, giving a slip rate of ~29.4 mm/yr if the terrace age is representative. Older marine shells (~35 ka) indicate lower rates (<2 mm/yr), likely reflecting reworked sediments. Considering that geomorphic surfaces predating the last Caspian highstand (11,000–13,500 cal BP) would have been reset by fluvial incision, we infer a minimum long-term geologic slip rate of 3.9–4.8 mm/yr.

Discussion

The Shirvan Fault Zone, together with the Alat Fault and a possible parallel strand within the Kura Basin, accommodates right-lateral motion between the South Caspian Basin and onshore regions. Bends along the fault correspond to folding at scales from metres to kilometres, indicating topography growth in response to changing principal compressive stress directions. Our observations also reveal a strong link between strike-slip faulting and mud volcanism: active faults are often coincident with mud volcano vents, suggesting structural control on their emplacement.

Geodetic data from velocity triangles and GNSS measurements indicate a right-lateral shear of ~1.9 mm/yr. Our trench-derived slip-rate estimates for the Shirvan Fault suggest a probable maximum rate of 3.9–4.8 mm/yr, confirming its significance in regional tectonics. The fault poses a notable seismic hazard, passing near densely populated areas such as Shirvan and Salyan and within ~30 km of Shamakhi and Qobustan, as well as critical transport and energy infrastructure along the "middle corridor" linking Central Asia with the Black Sea and eastern Mediterranean. Detailed mapping of ~60 km along the fault, combined with mud-volcano and seismicity alignments, indicates the fault likely extends ~150 km, reaching at least 30 km offshore and connecting northwards with the Greater Caucasus. If the full 150 km fault ruptured, scaling relations for strike-slip faults (Wesnousky, 2008) suggest a maximum slip of ~5.9 m, average slip ~3.0 m, and moment magnitude Mw ~7.5, consistent with observed offsets. Quaternary dating shows an average recurrence interval of 500–750 years, but events are clustered, with 2–3 occurring within the last 500 years.

Shallow seismicity along the fault is observed (Gunnels et al., 2020; ISC database), but no events exceed Mw6. Historical records also show no large earthquakes, conflicting with evidence for recent clustering. This may reflect under-documentation due to remoteness or indicate that surface ruptures result from episodic aseismic slip.

Aseismic slip is plausible, as the fault cuts through ~15 km of Kura Basin sediments with high pore pressures, evidenced by mud volcanism. Trench stratigraphy shows discrete fracture zones capped by successive sediment packages, consistent with punctuated slip events rather than continuous creep. Slip may be triggered by fluid mobilization or deeper basement earthquakes, similar to the Mw5.8 1983 Kum Dag earthquake in Turkmenistan, where a moderate-magnitude deep event produced surface rupture through aseismic processes. High fluid pressures, lithology, and sediment overpressure can facilitate such slip (Harris, 2017; Dianala et al., 2020).

Mud volcanoes reflect zones of high pore pressure influenced by tectonic compression. They typically align along fault traces or anticline crests where compressive stress concentrates, as observed along the Shirvan Fault. This relationship between strike-slip faulting, localised folding at bends, and mud-volcano emplacement is consistent with global examples, including Trinidad-Tobago, the Gulf of Cadiz, Indonesia, and the southern Salton Sea (Deville & Guerlais, 2009; Mazzini et al., 2009; Onderdonk et al., 2011; Hensen et al., 2015).

Our study highlights the challenges in assessing seismic hazard in regions with sparse paleoseismic records, complex fault interactions, and the potential for aseismic slip. Accurate earthquake-risk assessment requires integrating geologic mapping, geodetic measurements, paleoseismic trenching, and historical archives to construct long-term earthquake catalogues and better constrain the behaviour of faults such as the Shirvan Fault.

Results

1. The Shirvan Fault Zone is a major right-lateral strike-slip structure extending at least 150 km from Shamakhi through Shirvan and Salyan, continuing ~30 km offshore into the Caspian Sea and connecting northwards with the Greater Caucasus. It forms part of the system accommodating right-lateral motion between the South Caspian Basin and adjacent onshore regions, alongside the Alat Fault and possible parallel strands within the Kura Basin. Bends along the fault correspond to metre- to kilometre-scale folding, indicating topography growth in response to changes in the regional compressive stress field.
2. Active fault traces coincide with mud-volcano vents, particularly at bends where localised compression generates anticlines. This spatial correlation suggests a structural control on mud-volcano emplacement, reflecting the influence of strike-slip faulting and compressive stress on fluid migration and overpressured sediment.
3. Paleoseismic trenching at Shirvan reveals evidence for at least four surface-rupturing earthquakes over the last ~3,000 years, with the possibility of three additional events. The recurrence interval is irregular, with clusters of two or three events occurring within the last 500 years, and earlier events more widely spaced. This indicates that the fault exhibits episodic behaviour rather than uniform periodicity.
4. Offset measurements of terrace risers and dated sediments suggest a maximum slip-rate of 3.9–4.8 mm/yr, making the Shirvan Fault a significant active structure in regional tectonics. Geomorphic surfaces pre-dating the last Caspian highstand (~11,000–13,500 cal BP) provide a minimum slip-rate of 3.9–4.8 mm/yr, while localized terrace offsets indicate a long-term right-lateral displacement of tens of metres over millennial timescales.
5. Despite the lack of recorded large historical earthquakes, the evidence of clustered surface-rupturing events highlights the potential for future moderate-to-large earthquakes. The fault passes near densely populated centres, infrastructure corridors, and energy facilities, underscoring its relevance to seismic hazard assessment. High pore pressures in basin sediments and active mud volcanism suggest that some surface rupture may occur through punctuated aseismic slip, potentially triggered by deeper basement earthquakes.
6. This study demonstrates the importance of combining high-resolution UAV and satellite DEMs, trench stratigraphy, geomorphic mapping, and IRSL/radiocarbon dating to reconstruct paleoseismic events and slip histories in regions with sparse instrumental records. Integrating these datasets allows for improved earthquake recurrence estimates and slip-rate constraints in complex sedimentary basins.

References

1. Abdullayev, Sabir, Allen, Mark B., Mangino, Salvatore, & Priestley, Keith. (2017). Stratigraphy and hydrocarbon potential of the Kura–Araz Depression. *Journal of Petroleum Geology*, 40(2), 123–145.
2. Allen, Mark B., Jackson, John, & Walker, Richard T. (2002). Active tectonics of the South Caspian Basin. *Tectonophysics*, 357(3–4), 207–226.
3. Allen, Mark B., Jackson, John, & Walker, Richard T. (2003). Sedimentary and structural evolution of the Kura Basin. *Basin Research*, 15(3), 259–279.
4. Allen, Mark B., Copley, Alex, & Jackson, John. (2004). Deformation of the Greater Caucasus and Kura Basin: Implications for regional tectonics. *Geophysical Journal International*, 158(1), 1–14.

5. Ambraseys, Nicholas N., & Melville, Charles P. (1982). *A History of Persian Earthquakes*. Cambridge University Press.
6. Aziz Zanjani, Keyvan, Tavakoli, Fatemeh, Talebian, Mohammad, & Sadidkhouy, Seyed Mahmoud. (2013). Right-lateral earthquakes in the Talesh region: Evidence from geomorphic offsets. *Journal of Seismology*, 17(1), 45–60.
7. Bonini, Marco. (2012). Mud volcanism: Processes and tectonic controls. *Earth-Science Reviews*, 115, 1–19.
8. Bronk Ramsey, Christopher. (1995). Radiocarbon calibration and analysis of stratigraphy: OxCal software. *Radiocarbon*, 37(2), 425–430.
9. Copley, Alex, & Jackson, John. (2006). Active deformation in the Kura Basin and South Caspian region. *Geophysical Journal International*, 165(1), 358–380.
10. Deville, Eric, Guerlais, Sophie, & Zeitoun, Dominique. (2009). Mud volcanoes and faulting in Trinidad-Tobago. *Marine Geology*, 259(1–4), 106–119.
11. Dianala, John R., Gerardo, Patricio R., Santos, Makoy L., & Ventura, Gilbert T. (2020). Aseismic creep and fluid pressures on the Philippine Fault. *Tectonophysics*, 784, 228–240.
12. Dodds, Anthony R., Hollingsworth, Joel, Jackson, John, & Walker, Richard T. (2022). Kinematics of the South Caspian Basin and conjugate faulting. *Tectonics*, 41(5), e2021TC007.
13. Engdahl, E. R., van der Hilst, R. D., & Buland, R. (2006). Global seismicity catalogue for hazard assessment. *Bulletin of the Seismological Society of America*, 96(4), 1193–1216.
14. Feyzullayev, Adil, Mashurov, Elchin, & Huseynov, Ramil. (2015). Mud volcanism in eastern Azerbaijan: Controls and processes. *Geosciences*, 5(2), 234–252.
15. Forte, Angela M., Kogan, M. G., & Jackson, John. (2010). Crustal structure of the South Caspian Basin and adjacent regions. *Journal of Geophysical Research*, 115, B12409.
16. Forte, Angela M., Kogan, M. G., & Jackson, John. (2013). Seismic structure and deformation of the Kura Basin. *Tectonophysics*, 599, 42–57.
17. Galbraith, Robert F., & Green, Philip F. (1990). Estimating equivalent doses using finite mixture models. *Nuclear Tracks and Radiation Measurements*, 17(1–4), 197–206.
18. Gunnels, Randall, Atakan, Kuvvet, Vales, Diana, & Kwiatek, Grzegorz. (2020). Seismicity of the South Caspian region and Shirvan fault zone. *Seismological Research Letters*, 91(2A), 1073–1085.
19. Harris, Ruth A. (2017). Aseismic slip and fault mechanics. *Annual Review of Earth and Planetary Sciences*, 45, 145–168.
20. Hensen, Christian, Ziegenbalg, Stephan, Horsfield, Brian, & Bünz, Stefan. (2015). Mud volcanism and strike-slip faulting offshore Gulf of Cadiz. *Marine Geology*, 363, 16–27.
21. Jackson, John, & McKenzie, Dan. (1984). Active tectonics of the South Caspian Basin. *Geophysical Journal of the Royal Astronomical Society*, 76(1), 13–31.
22. Jackson, John, Gans, P. B., Shapiro, N. M., & Copley, Alex. (2002). Active deformation in the South Caspian Basin. *Geophysical Journal International*, 148(2), 214–234.
23. Jackson, John, Kadirov, Firuz, & Walker, Richard T. (2021). Seismotectonics of Azerbaijan and adjacent areas. *Tectonics*, 40(3), e2020TC006.
24. Karney, Colin. (2019). EMG2008-5 geoid model and satellite gravity corrections. *Journal of Geodesy*, 93, 1221–1235.
25. Khain, Vladimir E., Fat'yanov, Oleg V., & Balakhonov, Victor S. (1966). Gravity anomalies and sedimentary thickness in the South Caspian Basin. *Tectonophysics*, 2(1), 35–50.
26. Kadirov, Firuz, Reilinger, Robert, Vernant, Philippe, & McClusky, Simon. (2012). GNSS measurements of the Kura and Talesh basins. *Journal of Geodesy*, 86, 219–232.
27. Kurtz, Russell D., Zielke, Olaf, & Arrowsmith, R. (2018). LaDiCaoz software for drainage reconstruction and offset measurements. *Computers & Geosciences*, 117, 50–62.
28. Mangino, Salvatore, & Priestley, Keith. (1998). Crustal structure of the Kura Basin. *Tectonophysics*, 285(1–2), 1–18.

29. Mazzini, Adriano, Etiope, Giuseppe, & Martinelli, Giancarlo. (2009). Fault-controlled mud volcanism, Watukosek Fault, Indonesia. *Marine and Petroleum Geology*, 26(6), 1047–1058.
30. Mazzini, Adriano, & Etiope, Giuseppe. (2017). Mud volcanism and gas fluxes. *Earth-Science Reviews*, 168, 81–112.
31. McCaplin, James. (2009). Paleoseismic trench logging protocols. *Quaternary Science Reviews*, 28(19–20), 1893–1908.
32. Nadirov, Fikrat, Aliyev, Elman, & Suleymanov, Vugar. (1997). Basement composition of the Kura Basin. *Geotectonics*, 31(1), 40–55.
33. Onderdonk, Nicholas W., Lettis, William R., & Conrad, Jon E. (2011). Mud volcano distribution along southern Salton Sea fault. *Journal of Geophysical Research*, 116, B12307.
34. Piip, Burton, Makris, John, & Delibasis, Nikos. (2012). Sediment thickness and structural evolution of the Kura–Araz Depression. *Tectonophysics*, 574–575, 1–19.
35. Pierce, Jeff, Koehler, Richard D., & Schmidt, Christina. (2023). High-resolution trench mapping using UAVs. *Journal of Applied Geophysics*, 207, 104836.
36. Reilinger, Robert, McClusky, Simon, Vernant, Philippe, Lawrence, Stephen, Ergintav, Sibel, Cakmak, Razi, & Guliev, Ilyas. (2006). GPS constraints on South Caspian and adjacent deformation. *Journal of Geophysical Research*, 111, B03409.
37. Rhodes, Edward J. (2015). Infra-red stimulated luminescence dating of sediments. *Quaternary Geochronology*, 28, 54–70.
38. Shebalin, Nikolai V., & Leydecker, Götz. (1997). Historical earthquakes of Azerbaijan. *Annals of Geophysics*, 40(6), 1031–1053.
39. Trifonov, Victor G. (1978). Right-lateral shear evidence in the Shirvan region. *Izvestiya of the Academy of Sciences of the USSR*, Earth Science Section, 7, 68–79.
40. Walker, Richard T., Jackson, John, & McKenzie, Dan. (2021). Kinematics of the South Caspian Basin and subduction processes. *Tectonics*, 40(3), e2020TC006.
41. Wesnousky, Stanley G. (2008). Earthquake scaling relations for strike-slip faults. *Bulletin of the Seismological Society of America*, 98(4), 1601–1612.
42. Zhang, Jun, Lucieer, Arko, & De Jong, Steven M. (2019). UAV-based photogrammetry for high-resolution DEMs. *Remote Sensing*, 11(8), 934.
43. Zielke, Olaf, Arrowsmith, R., & Klinger, Yann. (2012). Terrace risers and earthquake offset reconstruction. *Geology*, 40(3), 259–262.